



A Fast Transient Absorption Study of $\text{Co}(\text{AcAc})_3$

Luisa Ferrari¹, Mauro Satta², Amedeo Palma³, Lorenzo Di Mario¹, Daniele Catone¹, Patrick O'Keeffe⁴, Nicola Zema¹, Tommaso Prosperi¹ and Stefano Turchini^{1*}

¹ CNR-ISM, Division of Ultrafast Processes in Materials (FLASHit), Area della Ricerca di Roma Tor Vergata, Rome, Italy,

² CNR-ISMN, Chemistry Department, Università di Roma Sapienza, Rome, Italy, ³ CNR-ISMN, Area della Ricerca di Roma 1 - Montelibretti, Rome, Italy, ⁴ CNR-ISM, Division of Ultrafast Processes in Materials (FLASHit), Area della Ricerca di Roma 1 - Montelibretti, Rome, Italy

The study of transition metal coordination complexes has played a key role in establishing quantum chemistry concepts such as that of ligand field theory. Furthermore, the study of the dynamics of their excited states is of primary importance in determining the de-excitation path of electrons to tailor the electronic properties required for important technological applications. This work focuses on femtosecond transient absorption spectroscopy of Cobalt tris(acetylacetonate) ($\text{Co}(\text{AcAc})_3$) in solution. The fast transient absorption spectroscopy has been employed to study the excited state dynamics after optical excitation. Density functional theory coupled with the polarizable continuum model has been used to characterize the geometries and the electronic states of the solvated ion. The excited states have been calculated using the time dependent density functional theory formalism. The time resolved dynamics of the ligand to metal charge transfer excitation revealed a biphasic behavior with an ultrafast rise time of 0.07 ± 0.04 ps and a decay time of 1.5 ± 0.3 ps, while the ligand field excitations dynamics is characterized by a rise time of 0.07 ± 0.04 ps and a decay time of 1.8 ± 0.3 ps. Time dependent density functional theory calculations of the spin-orbit coupling suggest that the ultrafast rise time can be related to the intersystem crossing from the originally photoexcited state. The picosecond decay is faster than that of similar cobalt coordination complexes and is mainly assigned to internal conversion within the triplet state manifold. The lack of detectable long living states (>5 ps) suggests that non-radiative decay plays an important role in the dynamics of these molecules.

Keywords: fast transient absorption, TDDFT (time-dependent density functional theory) calculations, femtosecond laser pulses, metal complexes, charge - transfer

OPEN ACCESS

Edited by:

Stefano Falcinelli,
University of Perugia, Italy

Reviewed by:

Nadja Doslic,
Rudjer Boskovic Institute, Croatia
Franco Vecchiocattivi,
University of Perugia, Italy

*Correspondence:

Stefano Turchini
stefano.turchini@ism.cnr.it

Specialty section:

This article was submitted to
Physical Chemistry and Chemical
Physics,
a section of the journal
Frontiers in Chemistry

Received: 07 February 2019

Accepted: 29 April 2019

Published: 21 May 2019

Citation:

Ferrari L, Satta M, Palma A,
Di Mario L, Catone D, O'Keeffe P,
Zema N, Prosperi T and Turchini S
(2019) A Fast Transient Absorption
Study of $\text{Co}(\text{AcAc})_3$.
Front. Chem. 7:348.
doi: 10.3389/fchem.2019.00348

INTRODUCTION

Transition metal complexes are of paramount importance in chemical and biological photochemical processes (Ruggiero et al., 2014) involving the conversion of the energy of visible light into chemical energy and the activation of redox-states for catalysis (Prier et al., 2013). Indeed, it is desirable to study the early formation of optically excited states, to explore the possibility of triggering and tailoring the electronic and structural properties of this class of compounds. Moreover, the spreading of the population of the excited electrons into different relaxation channels plays a key role in smart sensors and ultrafast devices (Wada, 2004).

The development of femtosecond laser sources gave rise to a revolution in the comprehension of the fate of excited electrons and provided a microscopic basis for already established theories such as molecular internal vibration relaxation (Grossmann, 2013), mostly based on the analysis of the photo fragmentation processes (Wada and Tanaka, 2013). Moreover, the advent of ultrafast X-ray facilities provided new insight into electronic and structural dynamics of transition metal complexes (Huse et al., 2011; Chergui, 2018). To this end future perspectives are strongly related to the ultrafast application of VUV-Soft X-ray PhotoElectron Spectroscopy studies in the gas phase, to our knowledge still lacking in the field of metal complexes, and the application of theoretical state of the art methods to characterize the dynamics of the electronic structure (Squibb et al., 2018).

The dynamics studies usually are modeled by excitation following the Franck-Condon approximation, which takes place in about 1 fs (Demtröder, 2008), then three different relaxation processes occur (Tramer et al., 2010). Internal conversion (IC) allows the de-excitation to a different electronic state within the same spin multiplicity. Intersystem crossing (ISC) is the mechanism characterized by a change of spin of the relevant electronic states. IC and ISC are first-order perturbation theory processes, their decay mode can be modeled by exponential functions and their rate is inversely proportional to the energy difference of the involved states (Bixon and Jortner, 1968). Vibrational cooling (VC), which is usually the fastest process, represents the de-excitation from the highest excited to the lower vibrational levels within the same electronic state; the decay is generally associated with energy dissipation toward the surrounding medium and can be modeled by perturbation theory using a bath Hamiltonian (Fujisaki et al., 2006).

Transition metal complexes present a manifold of low-lying excited states with a high density of states that enables them to efficiently harvest light; in a narrow interval of energy (hundreds of meV) the excited electronic states display different electronic character, inducing a great variety of de-excitation pathways and reactivity processes after optical excitation. Moreover, in transition metal compounds the spin-orbit coupling term of the Hamiltonian is strong because of the open d-shell of the metal and it favors a fast ISC with the subsequent formation of long living states. This is in contrast to organic molecules where ISC is generally slower than IC (Tramer et al., 2010). The strong spin-orbit term alters the hierarchy of the perturbations and makes the distinction between ISC and IC fuzziier. It is reasonable to assume that these two processes could occur in the same time scale and, consequently, convoluted, although in a quantum-mechanical picture the relative strength between the non-Born-Oppenheimer terms and the spin-orbit does not allow us to consider the two processes separated in terms of perturbation theory. The presence of ISC is generally associated with long living states that de-excite by phosphorescence decay.

The existence of two time scales related to fast and slow relaxation processes reflects different photochemical and photophysical phenomena. The fast evolution after photoexcitation displays intramolecular processes that dramatically change the electronic and structural properties in a very selective pathway; this can be tailored by tuning

the excitation energy and the vibrational composition of the excited state. On the other hand, relaxed fully thermalized excited states with lifetimes greater than the diffusion time scale provide the basis for slow photochemistry reactions that are not thermodynamically accessible in the ground state. Moreover, the electronic character of the excited states provides different chemical selectivity with respect to the ground state.

In metal complexes the tailoring of ISC by tuning the excitation channel can dramatically change the ratio between the fluorescence and phosphorescence relaxation channels (Hsu et al., 2012), with potential applications in sensor design.

The relevance of ISC in transition metal complexes dynamics has been extensively studied (Vlček, 2000; McCusker, 2003; Wagenknecht and Ford, 2011). Fluorescence up-conversion measurements on [Ru(bpy)₃]²⁺ display ISC for metal to ligand charge transfer (MLCT) states: ¹MLCT → ³MLCT with τ = 40 ± 15 fs, while IC displays a time scale of the order of picoseconds (Bhasikuttan et al., 2002). On the other hand, fast transient absorption spectroscopy (FTAS) measurements assign a τ ≈ 100 fs for the overall formation of the ³MLCT (Damrauer et al., 1997). [Fe(II)(tren(py)₃)]²⁺ shows ISC characteristic time constant less than 1 ps (Monat and McCusker, 2000). To establish the ⁵T₂ character of the long living state, the difference of absorption spectra of Fe(II) complexes with ⁵T₂ (high-spin) and ¹A₁ (low spin) ground state provided a reference for the time-resolved excited state spectrum. The assignment of ⁵T₂ to ¹A₁ conversion was recently found by a variable temperature FTAS study of [Fe(bpy)₃]²⁺-type complexes and [Fe(terpy)₂]²⁺ (Carey et al., 2019). FTAS studies on Co(III) compounds have been presented (McCusker et al., 1993): [Co(en)₃](ClO₄)₃, [Co(tpen)](ClO₄)₃, and [Co(tppn)](ClO₄)₃ show biphasic relaxation kinetics; in the case of [Co(tpen)]³⁺ excited-state decay is expressed by two time constants τ₁ = 4 ± 2 ps and τ₂ = 44 ± 5 ps, for [Co(tppn)]³⁺ τ₁ = 3 ± 1 ps and τ₂ = 51 ± 3 ps, while the data for [Co(en)₃]³⁺ give τ₁ = 2 ± 1 ps and τ₂ = 450 ± 100 ps. For [Co(tpen)](ClO₄)₃ and [Co(tppn)](ClO₄)₃ the experimental data suggest a lifetime of the ¹LMCT (ligand to metal CT) state less than 1 ps. No fluorescence yield was observed for the three compounds. Regarding the kinetics of the non-radiative decay, the relation between photochemical properties and ligand field excited state character leads to the assignment of the lowest lying excited state as ⁵T₂ for the octahedral Co(III) complexes considered. Cr(III)(AcAc)₃ has been thoroughly studied by means of FTAS (Juban and McCusker, 2005) and shows the formation of the ²E₂ state from LMCT and ligand-field excitation. The ligand field excitation presents a monophasic decay of τ₁ = 1.1 ± 0.1 ps for every excitation and pump wavelength, LMCT excitation exhibits τ₁ = 50 ± 20 fs and τ₂ = 1.2 ± 0.2 ps, associated with charge transfer to ligand field manifold ISC and VC to ²E₂, respectively. Transient infrared spectroscopy points out that 70-85% of the ground state population of Cr(acac)₃ recovers with a time constant of 15 ps, and the remaining population is described by the lifetime of the ²E state (Maçôas et al., 2007).

These results clearly indicate the action of fast intersystem crossing and reverse the usual sketch of ISC being the slowest process.

We present a FTAS study of Co(AcAc)₃, where AcAc is the Acetylacetonate molecule, a diketone moiety which forms complexes with transition metal atoms. This is a transition metal complex currently employed as a catalyst for the formation of C–C bonds and oxidation reactions (Ishii et al., 1996). This compound has closed shell with *D*₃ symmetry point group and allows reliable and accurate quantum chemistry calculations. The electronic structure of the molecule was characterized by photoelectron and circular dichroism photoelectron spectroscopy (Catone et al., 2012, 2013) with good agreement of theory with spectroscopic data.

By means of density functional theory (DFT) and time dependent density functional theory (TDDFT) quantum chemistry calculations, we provide a picture of the structural and electronic properties involved in the ultra-fast dynamics, discussing the ligand-field and the charge transfer states excitation. Ligand-field approach is very important for a qualitative assignment of electronic character and symmetry of excited states. DFT and TDDFT calculations provide a more precise characterization of the ligand to metal and metal to ligand excited states. FTAS data will be discussed in view of these results.

The aim of the present work is to investigate the interplay between ISC and the other relaxation processes on the basis of the calculated electronic structure and spectroscopic data.

EXPERIMENTAL DETAILS

FTAS is a pump-probe methodology that measures the difference in absorption between the excited state and the ground state taken at different time delays after the optical excitation at a defined wavelength.

The pump was generated by an optical parametric amplifier (OPA) fed by the 800 nm radiation of an amplified Ti:Sapphire laser with a pulse length of 35 fs and a repetition rate of 1 kHz, and the probe was a white light supercontinuum generated in a commercial transient absorption spectrometer (FemtoFrame II-IB photonics). The probe wavelengths ranged between 400 and 750 nm while the pump-probe delay time was scanned up to 100 ps, with an overall temporal instrument response function described by a Gaussian peak with FWHM of 50 fs. Co(AcAc)₃ (Sigma Aldrich, purity 99.99%) was diluted in acetonitrile (ACN). Two different concentrations were used in the pump-probe experiments on Co(AcAc)₃: 0.01 M (excitation wavelength 365 and 390 nm) and 0.05 M (excitation wavelength 580 and 650 nm). Typical pump laser fluence was 500–2500 μJ/cm². The measurements were carried out in a quartz cell with path length 1 mm. A blank pump-probe experiment was performed to seek non-linear contributions of the solvent in the experiment. We paid attention to minimize cross-phase modulation structures in the transient spectrum by choosing a suitable pump fluence, although for low pump absorption it was not possible to eliminate it completely. The chirp of the FTAS signal was corrected by an alignment based on a polynomial fit. Since the transient absorption slowly varies as a function of the wavelength, to increase the signal to noise ratio the temporal cuts were

averaged ±5 nm around the chosen wavelength. No FTAS signal was detected in the 800–1600 nm region of probe wavelength. Measurements were taken at the magic angle between the linear polarization vectors of pump and probe radiation. Further details of the experimental set-up can be found in previous publications (Catone et al., 2018; Fratoddi et al., 2018).

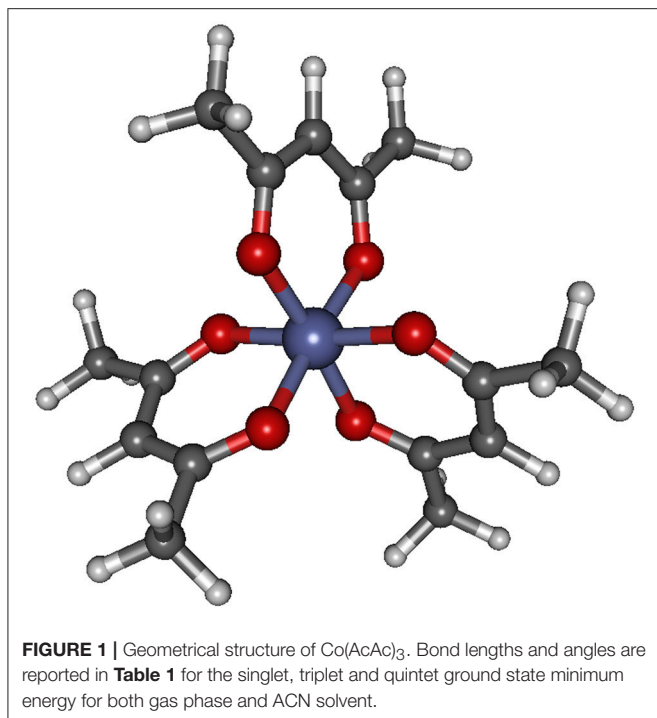
COMPUTATIONAL DETAILS

The description of the geometries and of the electronic structures of the gas phase and of solvated complex has been carried out using DFT formalism coupled with the polarizable continuum model (PCM) based on reaction field calculations and the integral equation formalism (Tomasi et al., 2005; Scalmani and Frisch, 2010). The excited states have been studied within the TDDFT approach (Bauernschmitt and Ahlrichs, 1996). The hybrid exchange-correlation functional Becke (Becke, 1993), three-parameter, Lee-Yang-Parr (Vosko et al., 1980; Lee et al., 1988; Stephens et al., 1994) has been adopted together with the split-valence double-zeta Pople basis set (Hariharan and Pople, 1973; Francl et al., 1982) with the addition of extra functions as established by Barone et al. (Barone et al., 2008) to be used in the frame of effective discrete/continuum solvent models. TDDFT and the chosen basis set are a good compromise between accuracy and computer time consuming for these complexes. TDDFT with B3LYP has been successfully used in the literature to characterize the electronic structure in similar calculations (Savarese et al., 2012, 2014; Catone et al., 2018).

The geometries were fully optimized for the ground states of the singlet, triplet and quintet spin configurations; at each of these geometries the first twenty excited electronic states have been computed. In order to have a picture of the excitation of the singlet, triplet and quintet states during the vertical transition from the initial geometry of the ground state, we have calculated the singlet, triplet, quintet excited electronic levels at the singlet minimum energy geometry. All the calculations were performed using the Gaussian code (Frisch et al., 2016).

The ISC processes have been described by estimating the relative non-radiative lifetimes computed by means of spin-orbit coupling matrix elements. In particular, we have used ADF (2018) code to calculate the spin-orbit coupling as a perturbation to a scalar relativistic calculation of TDDFT excitation energies for the gas phase. The TDDFT has been performed using the B3LYP functional, in analogy with our results obtained by Gaussian code, with double zeta polarization basis set on H, C, and O atoms, whereas the Co basis set is double zeta with 1s, 2s, 2p frozen core.

The number of singlet excited states considered was 20 for the singlet, and 60 for the triplet due to degeneracy. The spin-orbit coupling matrix was computed at the geometry corresponding to vertical transition from the equilibrium geometry of the electronic ground state. Several unsuccessful attempts to follow the geometry relaxation of the singlet electronic excited states were performed resulting in several singlet-singlet crossings along the optimization paths which at the end always lead to the first singlet excited state. The spin-orbit coupling matrix was



computed at five different geometries only for the first singlet excited state, taking the geometries from the optimization of the first singlet excited state performed by Gaussian code.

The ISC non-radiative lifetimes τ_i^{NR} , where i is the i th singlet excited state, have been computed following the Fermi golden rule with a Franck-Condon weighted density of states (FCWD), which assumes an equal vibrational structure between the involved electronic states (Valiev et al., 2018):

$$1/\tau_i^{NR} = \frac{2\pi}{\hbar} \sum_j \text{SO}_{ij}^2 \frac{\Gamma}{(\Delta E_{ij}^2 + \frac{\Gamma^2}{4})}$$

with the relaxation width of the vibronic levels Γ taken as 10^{14} s^{-1} , which is a condition generally fulfilled in experimental studies of luminescence properties (Valiev et al., 2018), SO_{ij} are the spin-orbit matrix element coupling the i th singlet state with the j th triplet state, and ΔE_{ij} is the corresponding energy difference.

RESULTS AND DISCUSSION

The structure of the Co(AcAc)₃ complex is shown in **Figure 1**, while the most significant geometrical parameters are reported in **Table 1** for the minimum energy geometries of the three spin configurations.

It is worth noting that while in the singlet and quintet configuration the three rings are all planar and the symmetry of the system remains D_3 , in the triplet case one of the rings is bent (C-O-Co-O 25.1° and 25.0° for the gas phase and ACN solvent, respectively) lowering the symmetry of the system. The minor changes in the geometrical parameters reported in **Table 1** for

the three different spin configurations should take place during the ISC relaxation dynamics following the initial excitation. In the case of the gas-phase complex the calculations show (see **Figure 2**) that the triplet ground state is about 1 eV above the singlet ground state, while the quintet ground state is slightly higher than the triplet state. For the triplet spin configuration (right part of **Figure 2**) the energy level distribution is quite uniform: about 20 levels in an energy interval of 3 eV. In contrast, for the quintet spin case (left part of **Figure 2**), there is an energy gap of about 2 eV between the ground and first excited state, above which there is a quite uniform distribution of the density of states (DOS) up to 5.5 eV. In order to have a qualitative picture of the dynamics involving ISC, we report the singlet, triplet and quintet excited energy levels calculated at the geometry of the singlet ground state minimum energy (central part of **Figure 2**). In the energy gap between the first singlet excited state and the ground state energy (about 2 eV), there are several other energy levels of the triplet and quintet states. An analogous quite high DOS is calculated up to 5 eV above the ground singlet state, thus supporting the possibility of a complex intersystem evolution of the wavepacket produced by the initial vertical photo-excitation.

In the ACN solvent (see **Figure 3**) the quintet ground state minimum energy is lower than that of the triplet, and it is about 0.8 eV above the singlet ground state. The DOS for the singlet, triplet and quintet states are similar to each other, in particular the DOS calculated in the geometry of the singlet ground state minimum energy are quite similar to those calculated in the gas phase, while for quintet the density of state changes significantly. The large difference between the quintet energy calculated in the gas phase and ACN is related to the high polarizability of these spin states with respect to triplets and singlets.

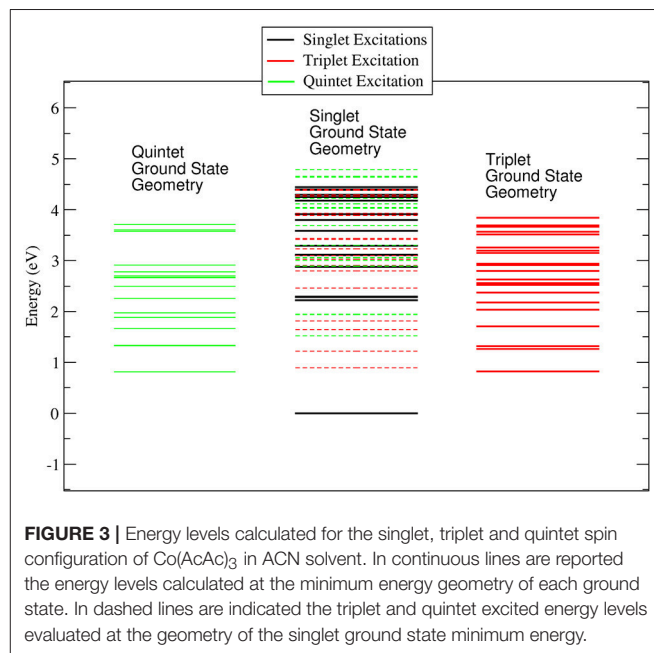
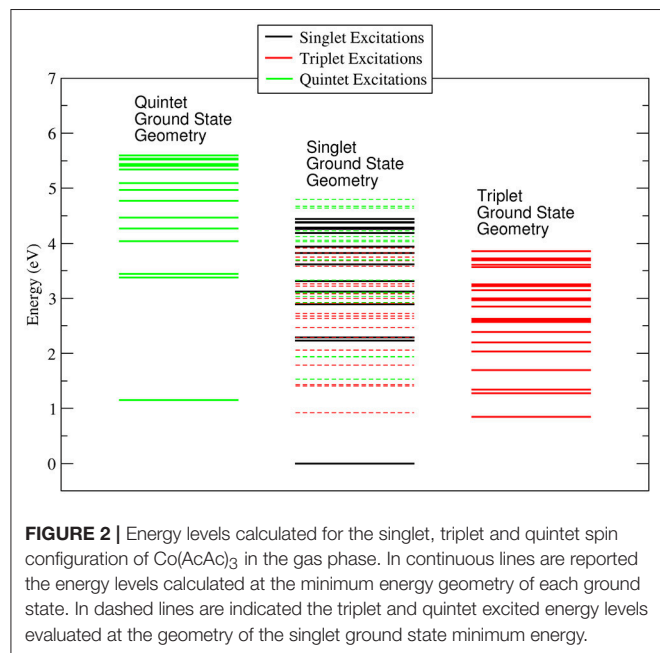
The electronic scheme of octahedral metal complexes is ruled by ligand field splitting of the d electrons. Tanabe-Sugano d^6 diagrams assign 1A_1 character to the ground state, with excited states in order of energy 3T_1 , 3T_2 , 1T_1 (Griffith, 1961). The energy of the 5T_2 with respect to singlet and triplets states depends on the ratio Δ/B of the crystal field parameters, where Δ is the octahedral energy splitting and B the Racah electron repulsion parameter. **Figure 4** reports the one electron picture of the 1A_1 , 3T_1 , 5T_2 octahedral ligand field states along with the excited states involving the ligand. The D_3 point group symmetry splits the above octahedral states, however in this work we shall relate each state to the original octahedral symmetry in order to simplify comparison with the literature.

Figure 5 reports the experimental absorption of Co(AcAc)₃ along with the theoretical oscillator strength calculations in ACN. The spectrum shows a broad band centered at 2.1 eV, where the d-orbital excited states of the Co are relevant, and a steep rise starting at 2.4 eV, associated with the LMCT manifold. **Table 2** displays the TDDFT excitation energies, the irreducible representations and oscillator strengths calculated for ACN; the numeric label in the table will be used in the discussion to identify the states. In order to have a good agreement with the experiment a rigid shift of 0.2 eV toward lower energies is applied to the calculated data. This shift value is compatible with the accuracy of

TABLE 1 | Most significant geometrical parameters for the singlet, triplet and quintet ground state minimum energy and first excited state singlet level for Co(AcAc)₃ in the gas phase and in ACN solvent.

	Gas phase				Acetonitrile			
	Ground state singlet	Ground state triplet	Ground state quintet	First excited state singlet	Ground state singlet	Ground state triplet	Ground state quintet	First excited state singlet
Co-O	1.91	2.03–1.91	2.01	1.91–2.08	1.91	1.90–2.07	2.01	1.91–2.07
O-Co-O _(ring)	95.2	88.4–93.4	86.3–86.4	89.8–93.9	95.2	88.1–93.6	86.4	88.1–93.6
C-O	1.27	1.26–1.27	1.27	1.26–1.27	1.27	1.27–1.28	1.27	1.27–1.28
C _{sp2} -C _{sp2}	1.40	1.41	1.40	1.41	1.40	1.41	1.40	1.40–1.41
C _{sp2} -C _{sp3}	1.51	1.51	1.51	1.51	1.51	1.51	1.51	1.51
C-O-Co-O	0.0	4.5–25.1	0.5–1.0	1.0–21.8	0.0	7.5–25.0	0.5–1.8	7.1–26.5

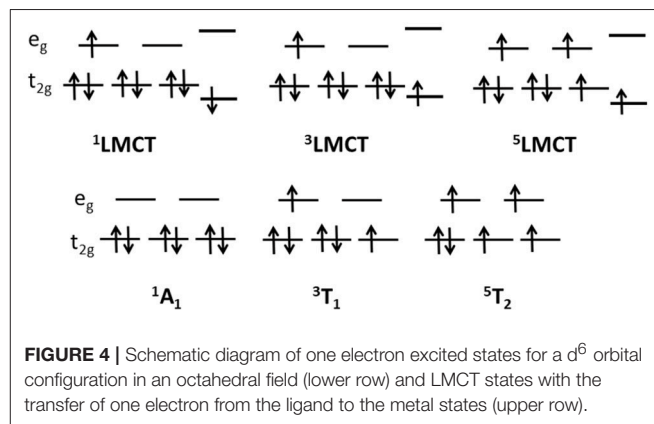
Distances in Angstrom, angles in degrees.



the TDDFT method. The oscillator strengths of quasi-degenerate states have been summed.

In the photon energy range 1.8–2.7 eV the envelope of d-d transitions is reproduced by the transition to excited states 1–3. The octahedral ¹T₁ state is split by the D₃ symmetry group into an A state (1) and double degenerate E states (2,3) at calculated excitation energies 2.23 and 2.29 eV, respectively. The charge transfer states ¹LMCT are represented by an A state at 2.88 eV (4), associated with zero oscillator strength, and a pair of doubly degenerate E states at 3.11 eV (5,6) and 3.28 eV (7,8), respectively.

The excitation (¹A₁ → ¹LMCT) produces a marked ligand-to-metal character for the complex both in the gas phase and solvated in ACN, as **Figure 6** shows (excitation at 5 (3.11 eV), 6 (3.11 eV), 7 (3.29 eV), 8 (3.29 eV) in ACN), where there is a charge transfer from the three organic ring molecules of AcAc to the cobalt central atom. This electronic rearrangement does not invert the net charge transfer which occurs in the ground state of the metal complex, where about 0.5 e of charge is transferred from



the metal atom to the ligands. The yellow iso-density surfaces represent an enrichment of the electron charge density upon excitation, whereas the blue iso-surfaces indicate a depletion

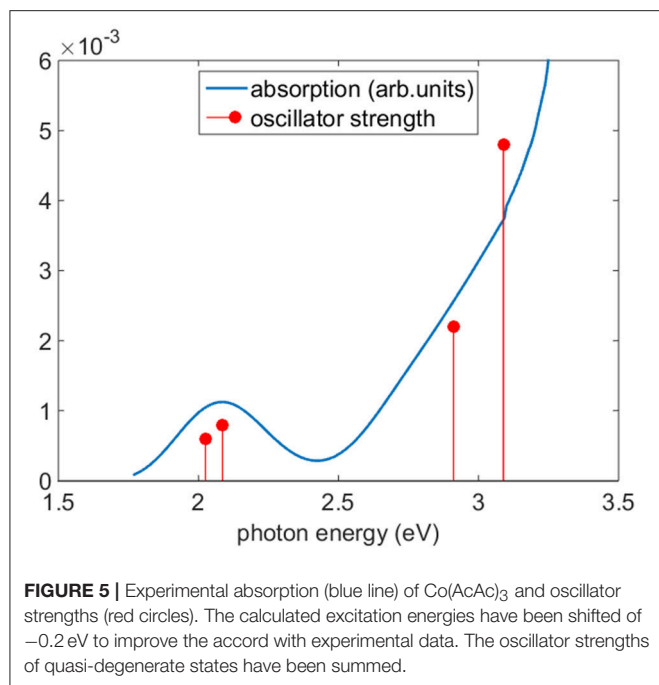
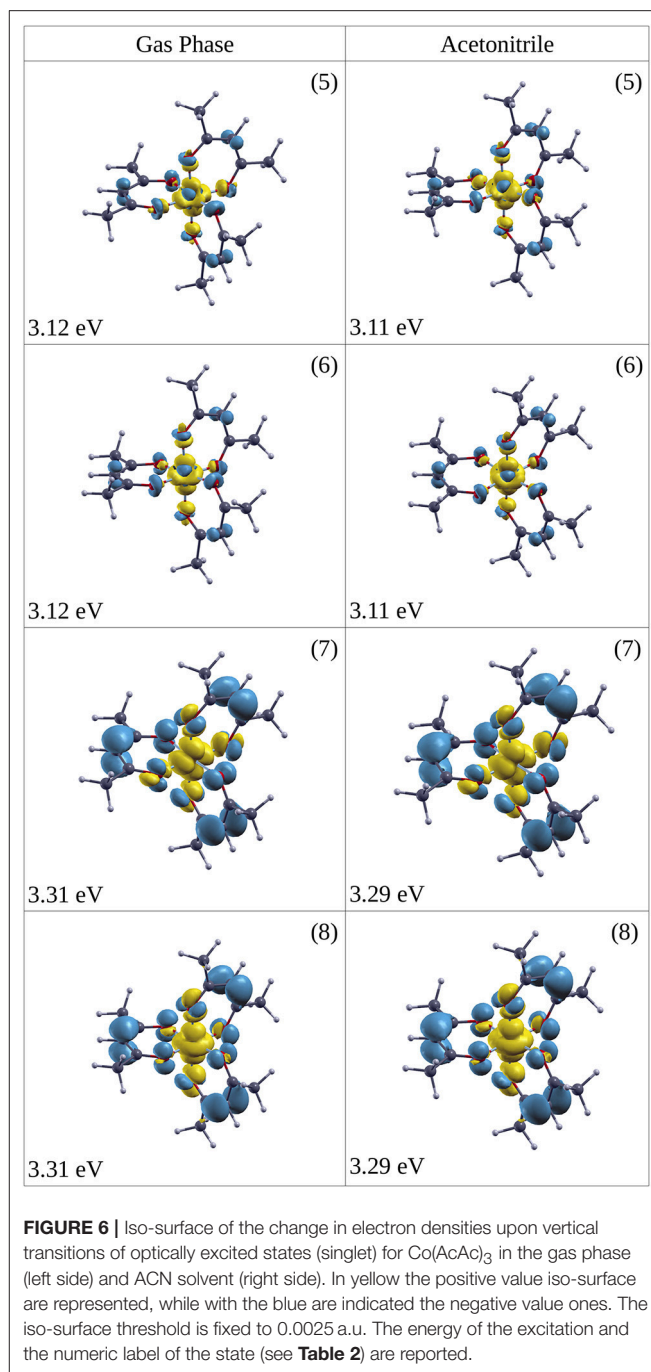


TABLE 2 | Theoretical transition energies, wavelengths and oscillator strengths of optically excited states for Co(AcAc)₃ in ACN.

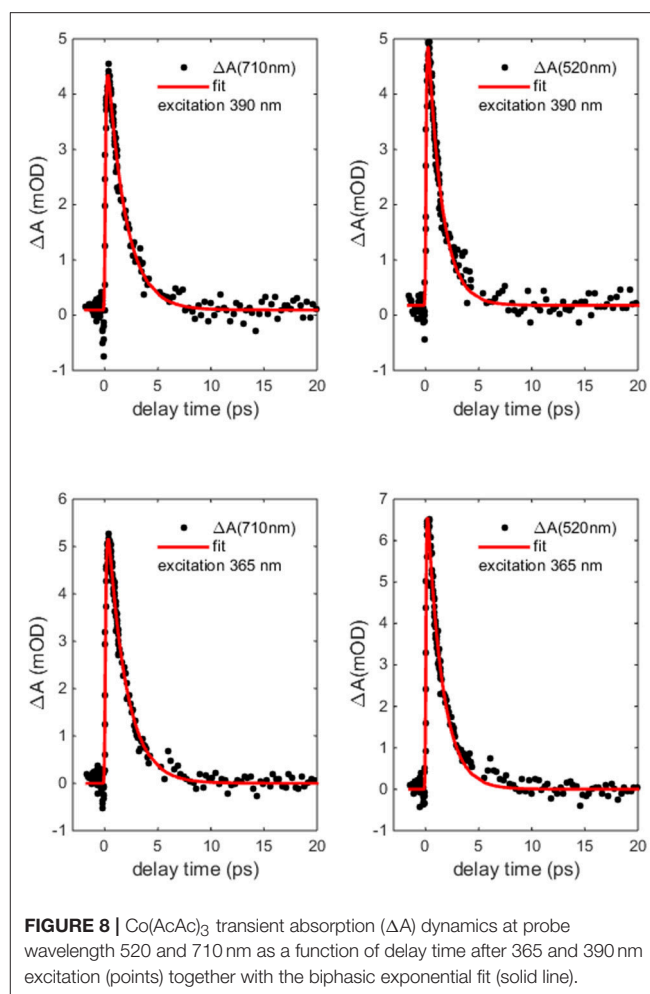
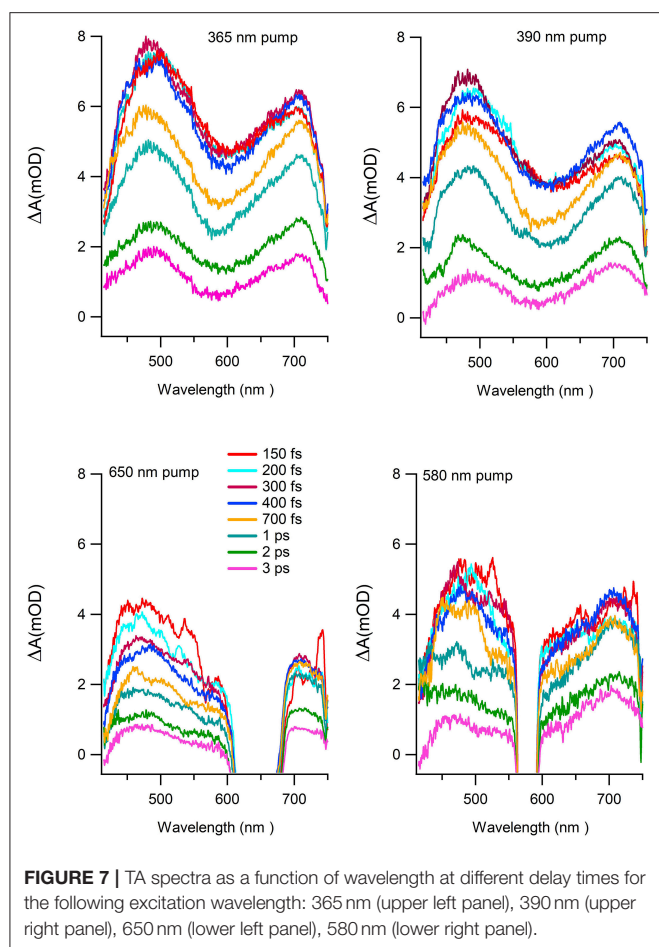
Excited state (Singlet)	Symmetry	Energy		Oscillator strength
		(eV)	(nm)	
1	1 ¹ A	2.2250	557.23	0.0006
2	1 ¹ E	2.2854	542.51	0.0004
3	1 ¹ E	2.2876	541.98	0.0004
4	2 ¹ A	2.8762	431.07	0.0000
5	2 ¹ E	3.1103	398.62	0.0011
6	2 ¹ E	3.1118	398.43	0.0011
7	3 ¹ E	3.2884	377.04	0.0024
8	3 ¹ E	3.2916	376.66	0.0024
9	3 ¹ A	3.5876	345.59	0.0000
10	4 ¹ E	3.7985	326.40	0.0001

in the electronic charge density, as reported in **Figure 6**: in particular there is a rearrangement of the electron charge density over the p MOs of the oxygen atoms, while the CH groups are net charge donors during this electronic transition with a reduction in the p MOs charge density. The excitation at 3.11 eV (399 nm) produces a charge electron density shift from the rings to a d_{z^2} MO of the central Co atom both in the gas phase and in the ACN solvent (see **Figure 6**). In one case of excitation at 3.29 eV (excitation 7 in **Table 2**) the charge density is shifted into a d_{xy} MO of Co, while in the other excitation at 3.29 eV (excitation 8 in **Table 2**) the density shift is from the ring to a d_{z^2} MO of Co. The amount of the charge density shift is higher in the transition at 3.29 eV (377 nm) with respect to that at 3.11 eV (399 nm). Since it is difficult to exactly locate the energy position of the



¹LMCT in the experimental spectrum, we chose two wavelengths for the pump to excite electronic states with reasonable excess energy: 5 and 6 at 390 nm (photon energy 3.18 eV) and 7 and 8 at 365 nm (photon energy 3.40 eV). For the excitation of the ligand-field state two wavelengths were chosen for the pump: 580 nm (2.13 eV) near the maximum of the ligand-field state absorption and 650 nm (1.91 eV) at the onset of the absorption curve.

Figure 7 reports the transient absorption (TA) spectra (ΔA in the figure) in the 400–750 nm probe wavelength range at different delay times after the excitation at the chosen wavelength. The



spectra taken at 365 and 390 nm (**Figure 7** upper panels) display similar shape and time dependent behaviors. The TA spectra show positive values associated with a dominant contribution of the excited state absorption and two clearly defined broad bands, approximately centered at 480 and 700 nm. Two distinct time dependent regimes can be identified by analyzing the temporal evolution. Although the bands do not evolve in shape and wavelength position as a function of time, there is a clear evolution in their branching ratio. In the time range 0.1–1 ps the branching ratio between the maxima of the two structures monotonically decreases from roughly 1.3 to 1 and remains almost constant for $t > 1$ ps. The change in absorption suggests that the formation time of the population of the electronic state, which decays to the ground state, is about 1 ps. The lack of the appearance of new structures and of meaningful shifts of the maxima, together with the recovery of the kinetic traces back to $\Delta A = 0$, are strong indications that the molecule preserves its electronic structure and no photodegradation occurs. The dynamics of the Co(AcAc)₃ fades out at about 5 ps and long living state are absent at every pump wavelength employed. **Figure 8** reports the time evolution of the TA spectra at fixed probe wavelengths (520 and 710 nm) as a function of the delay time for excitations at 365 and 390 nm. The cuts are characterized by a swift rise, clearly

revealed within the temporal resolution of the pump-probe system.

The curves were fitted with a biphasic exponential function one related to the ultrafast rise time and the other related to the slower picosecond relaxation process. In the fit the temporal instrument response function (50 fs) was taken into account. In **Table 3** the time constants of the two processes are reported as a function of selected probe energies around the maxima of the two broad structures. For both pumps at 365 and 390 nm the time constants only very weakly depend on the probe wavelengths and substantially agree within the fit error. For the 390 nm excitation the averaged fit values are $\tau_1 = 0.08 \pm 0.04$ ps for the rise and $\tau_2 = 1.5 \pm 0.3$ ps for the decay, and for 365 nm excitation the value are $\tau_1 = 0.07 \pm 0.04$ ps and $\tau_2 = 1.5 \pm 0.3$ ps.

We now connect the phenomenological data analysis to a model of the dynamics of the Co(AcAc)₃ LMCT excited states and assign the hierarchy of the processes governing the dynamics of the molecule excitation. According to the literature ISC is the most likely fastest process. A previous FTAS study of Co(III) compounds (McCusker et al., 1993) proposed two mechanisms to understand the possibility to access different spin configurations. The first mechanism is ISC, while the second one points out that the LMCT transition alters the charge of the Co(III) ion that

TABLE 3 | Lifetimes after 365, 390, 580 and 650 nm excitation at selected probe wavelengths.

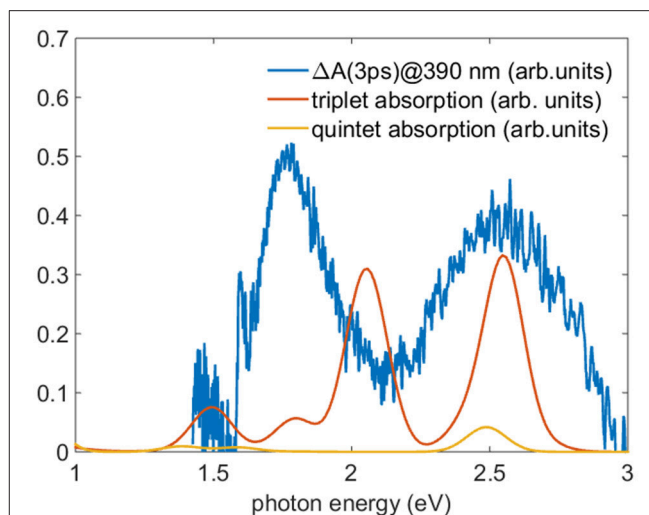
Pump wavelength (nm)	Probe wavelength (nm)	τ_1	τ_2
		(ps)	(ps)
365	460	0.08 ± 0.04	1.5 ± 0.2
	520	0.04 ± 0.04	1.3 ± 0.2
	680	0.08 ± 0.04	1.6 ± 0.2
	710	0.10 ± 0.04	1.7 ± 0.2
390	460	0.10 ± 0.04	1.5 ± 0.2
	520	0.06 ± 0.04	1.2 ± 0.2
	680	0.07 ± 0.04	1.7 ± 0.2
	710	0.10 ± 0.04	1.7 ± 0.2
580	460	-	1.6 ± 0.2
	520	-	1.6 ± 0.2
	680	0.06 ± 0.04	2.0 ± 0.2
	710	0.07 ± 0.04	2.1 ± 0.2
650	460	-	1.7 ± 0.2
	520	-	1.3 ± 0.2
	680	-	-
	710	0.07 ± 0.04	2.1 ± 0.2

τ_1 and τ_2 are related to the lifetime of the rise and of the decay of the photoinduced absorption at the indicated wavelength, respectively. The rise is within the temporal resolution after 580 and 650 nm excitation for the 460 and 520 nm probe wavelength. After 650 nm excitation at the probe wavelength of 680 nm the fit of the lifetime was not possible due to the residual intensity of the pump.

assumes a Co(II) character. Due to known instability of Co(II) low-spin states the metal ion could provide a swift transition low-spin → high-spin. Both processes lead to the same final state: in the former case the mechanism has a molecular nature, in the latter is based on the metal ion.

In view of these results we suggest that the origin of the rise time lies in an ISC that takes place on time scale of the order of tens of fs (Bhasikuttan et al., 2002) which depopulates the ¹LMCT in favor of different spin states. The sum of the manifold of these processes gives rise to the phenomenological fast onset. It is worth noticing that the variety of the states involved causes different probed dynamics that is reflected in the slightly different response of the states to the photon energy of the probe pulse. Hence the spread of the τ_1 values is related to the time scale of the different dynamics of the population of the states composing the early dynamics of ISC.

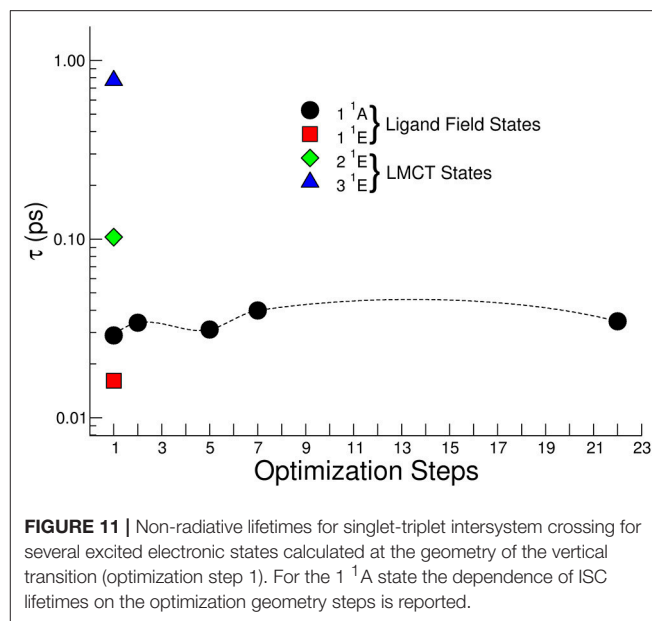
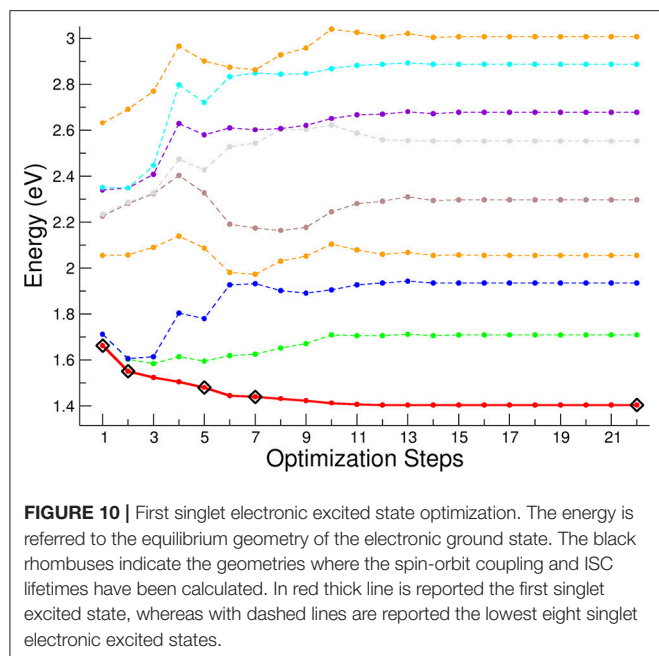
To test the hypothesis of the population of the lowest triplet and quintet levels, we compare the TA spectra after a time delay greater than 2 ps with the TDDFT calculations of the absorption spectra of the lowest energy levels of triplet and quintet states. **Figure 9** reports the calculated spectra of triplet and quintet lowest states together with the experimental TA spectrum measured 3 ps after 390 nm excitation. The oscillator strengths are converted into absorption by convolution with a gaussian function with a standard deviation of 100 meV. In the comparison a rigid shift of 300 meV toward lower photon energies was applied. There is a clear accord in the branching ratio between the two most intense triplet transitions

**FIGURE 9** | Comparison between the TA spectrum acquired 3 ps after the 390 nm excitation (blue line) and the TDDFT calculated absorption in acetonitrile of the lowest level of the triplet (red line) and quintet (yellow line). To reproduce the absorption the oscillator strength were convoluted with a gaussian function with standard deviation of 100 meV and the energy of the theoretical calculation shifted of 300 meV toward lower energy.

and the experimental curve. Although the absolute energy is slightly miscalibrated and the lack of vibrational calculations hinders the comparison, the energy difference of the calculated triplet transitions is 0.5 eV where the experimental energy difference between the experimental bands is about 0.7 eV, with a reasonable accord taking into account the accuracy of the TDDFT. This result sheds light on the process of the formation of the population of the states stemming from ISC suggesting the assignment of a predominant triplet character to the TA spectrum. According to these calculations, in the energy range investigated (1.5–3 eV) the ground state quintet oscillator strengths are one order of magnitude less favored than those of the triplets, and hence TA spectra are less sensitive to quintet transitions contributions. For this reason the presence of population in the quintet lowest level cannot be excluded.

VC occurs on the same time scale as the ISC and should be considered in the formation of the triplet (quintet) state. In the case of Co(AcAc)₃, according to DFT calculations, the ground states of triplet and quintet states present an elongation of the Co–O bond length in the interval 0.1–0.2 Å associated with a lower symmetry with respect to the octahedral coordination. The elongation of the R_{Co-O} bond length is then related to the fastest processes. A similar elongation is found by means of X-ray TA for Fe–N bond of [Fe^{II}(mbpy)₃]²⁺ in acetonitrile for the photoinduced high spin (HS) ⁵T₂ state (Liu et al., 2017).

In order to study the relaxation following the excitation processes, we have reported the geometrical optimization of the first singlet excited state in **Figure 10**. The higher energy curves (shown as colored lines) refer to higher singlet electronic states. The optimization steps corresponding to the sample geometry structures used to compute the spin-orbit coupling matrix and ISC lifetimes are shown as rhombuses. Here, the



first point of the optimization steps represents the vertical excitation corresponding to the geometry of the equilibrium structure of the ground singlet state. It can be seen that the initial degeneracy, associated with the D_3 symmetry, is removed during the relaxation path. After the 7th point of the optimization steps the energy remains almost constant, with a variation less than 30 meV with respect to the asymptotic energy corresponding to the equilibrium structure of the first excited singlet state. The higher energy singlet curves have a complex behavior along the relaxation path, and are characterized by several crossings, which open the way to a non-radiative decay by conical intersection from the singlet high energy states toward the lower excited singlet states.

Figure 11 reports the calculated lifetime τ for the singlet – triplet ISC of the optically active first four singlet excited states calculated at the geometry of the vertical transition (step 1 in **Figure 11**). Only for the 1^1A state the dependence of ISC lifetimes on the optimization steps is reported. The 1^1A ISC lifetime weakly depends on the optimization step and beyond step 7 there is no substantial change in the geometry of the complex, and consequently the change in the spin-orbit coupling matrix is negligible. It is worth noticing that for the excited states corresponding to the LMCT the τ related to the vertical transition geometry is within the range 0.1 – 1.0 ps, while in the ligand field case is faster and presents values in the range 0.01–0.02 ps.

The ISC calculations performed offer a quantitative basis for the analysis of the experimental lifetimes.

The fast experimental lifetime $\tau_1 = 0.08 \pm 0.04$ ps after excitation at 390 nm is in good agreement with that expressed by the 2^1E state about 0.1 ps, suggesting a fast singlet-triplet ISC.

The 3^1E state presents a τ about 1 ps at the geometry of the vertical transition and the measured lifetime $\tau_1 = 0.07 \pm 0.04$ ps at 365 nm suggests an IC transition toward the first excited singlet state and then a fast ISC with lifetime about 20 fs from 1^1A .

However, we cannot exclude a fast geometry relaxation on this particular electronic state that lower the ISC lifetime to tens of fs. The dynamics expressed by the time constant τ_2 contains the last part of the dynamics, the relaxation toward the lowest levels of the triplet state and, successively, to the ground states. Although, as explained above, the excited states populated with the pumps at 390 nm and 365 nm present a different interpretation in the dynamics, the information condensed in the time constants does not present a difference within experimental error.

The proposed dynamics is summarized in the Jablonski diagram reported in **Figure 12**, where the relaxation paths of 1LMCT (2^1E) and 1LMCT (3^1E) are shown.

To complete the study of the dynamics with excited states associated to the ligand-field excitation, the same analysis was performed for pump wavelengths of 580 and 650 nm. The spectral features of the absorption difference, plotted at different delay time (**Figure 7** lower panels), have a comparable behavior with the 390 and 365 nm analysis; two broad bands are present and positive values in the investigated range. In particular, the TA spectra measured after 580 nm excitation exhibit the same qualitative evolution of the branching ratio of the LMCT excited spectra for a time delay greater than 2 ps. For the spectra obtained with a pump at 650 nm the branching ratio analysis is hampered by the presence of the residual pump signal. However, the band at lower wavelength appears to be extended toward the blue with respect to the LMCT case. **Table 3** reports the time constants of the two processes as a function of selected probe energies for pump wavelengths of 580 and 650 nm, respectively. It is worth noticing that the fast rise measured in the previous case ($\tau_1 = 0.07 \pm 0.04$ ps) is observed only in the band centered at about 700 nm, while it is within the temporal resolution of the experimental system in the band in the range 450–600 nm.

At excitation wavelength of 580 nm the slow lifetime constant associated to the averaged fit values is $\tau_2 = 1.6 \pm 0.2$ ps for the low wavelength band (450–600 nm) and $\tau_2 = 2.0 \pm 0.2$ ps for the

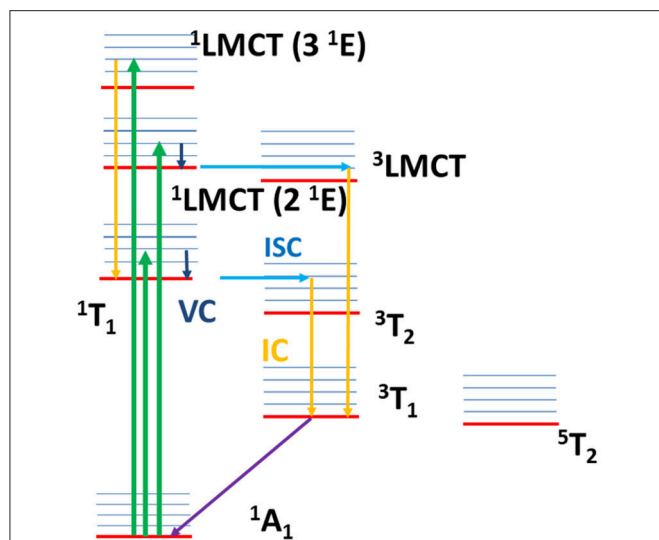


FIGURE 12 | Jablonski diagram with the sketch of the excited state dynamics. The arrows explain qualitatively the dynamics: absorption transitions (green arrows), internal conversion (yellow arrows), intersystem crossing (light blue arrows), vibrational cooling (dark blue arrows), non-radiative decay toward the ground state (violet arrow). After ligand field excitation (1T_1), VC and ISC occur with an overall lifetime 0.07 ± 0.04 ps and, successively, IC toward the lower triplet state and relaxation toward the ground state with a lifetime 1.8 ± 0.3 ps. The same dynamics is proposed for the $^1LMCT(2^1E)$ excitation, with VC and ISC ($^1LMCT \rightarrow ^3LMCT$) overall lifetime 0.08 ± 0.04 ps, and IC and non-radiative relaxation overall lifetime 1.5 ± 0.3 ps. For $^1LMCT(3^1E)$ excitation the calculations assign an ISC lifetime about 1 ps, slower than the experimental rise time 0.07 ± 0.04 ps. A fast IC toward the first singlet excited state and a fast singlet-triplet ISC is suggested to be associated with the fast experimental lifetime. The decay toward the ground state is sketched by IC within the triplet states and non-radiative decay with lifetime 1.5 ± 0.3 ps.

high wavelength band (650–750 nm). For excitation at 650 nm the averaged lifetime constants are $\tau_2 = 1.5 \pm 0.2$ ps and $\tau_2 = 2.1 \pm 0.2$ ps for the low and high wavelength bands, respectively.

It is impossible to disentangle the decay time constant of the two relaxation channels and we assign an overall averaged value to the decay time constant in the ligand field excitation case $\tau_2 = 1.8 \pm 0.3$.

The calculated singlet – triplet ISC τ for the ligand field states is in the range of 10 – 20 fs and confirms this phenomenological picture. In the low wavelength band the rise time is faster than the time resolution of the system and is compatible with an ISC of few tens of fs, while the high wavelength band probably contains information about VC relaxation.

The relaxation channels above discussed are reported in the Jablonski diagram in **Figure 12** (1T_1 excitation).

Comparing the results obtained in this study on $\text{Co}(\text{AcAc})_3$ with the $\text{Cr}(\text{AcAc})_3$ (Juban and McCusker, 2005) case, the

REFERENCES

- ADF. (2018). *SCM, Theoretical Chemistry*, eds E. J. Baerends, T. Ziegler, A. J. Atkins, J. Autschbach, O. Basergio, D. Bashford, et al. (Amsterdam: Vrije Universiteit). Available online at: <http://www.scm.com>
- Barone, V., Cimino, P., and Stendardo, E. (2008). Development and validation of the B3LYP/N07D computational model for structural parameter and

dynamics of these molecules exhibits similar time constants and interpretations. Indeed, the order of magnitude of the time scale of the ISC presents a slight dependence on the different electronic and spin character of the transition (quadruplet to doublet in $\text{Cr}(\text{AcAc})_3$ and singlet to triplet in $\text{Co}(\text{AcAc})_3$).

CONCLUSIONS

The FTAS study of $\text{Co}(\text{AcAc})_3$ displayed a very fast de-excitation dynamics characterized by a distribution of processes with lifetime constants on the scale 1–2 ps.

On the grounds of the TDDFT analysis we identified different processes associated with these dynamics. An elongation of Co–O bond length with reduction of octahedral symmetry subsequent to the LMCT excitation can be associated with the early stage of dynamics. The transient absorption spectra for delay times greater than 2 ps reveal the features of the absorption of the lowest triplet state. It is worth noticing that the findings of TDDFT theory can help to connect the phenomenological analysis to a microscopic model. A TDDFT calculation and a parametrized model was used to calculate singlet-triplet ISC lifetime at the vertical geometry, with values in the range 10–20 fs for LF states and 0.1–1 ps for LMCT states.

To summarize the dynamics, the formation of the population of the triplet involves different concomitant processes, such as vibrational relaxation, geometry distortion, intersystem crossing. The microscopic processes included in the fast time constant are the vibrational cooling and the intersystem crossing, while the slower lifetime decay involves the journey toward the lowest triplet state and the final relaxation to the ground states.

We believe that the characterization of the dynamics of metal complexes is desirable in view of possible spintronic applications that nano-fabrication could provide. The LMCT fast de-excitation with a short transient in the triplet state could be exploited in single molecule devices such as spin-valves.

AUTHOR CONTRIBUTIONS

MS and AP performed the theoretical calculations. The remaining authors performed the experiments and the data analysis. All the listed authors equally contributed to the scientific discussion and the writing of the manuscript.

ACKNOWLEDGMENTS

We gratefully acknowledge the support of NVIDIA Corporation with the donation of the Titan V GPU used for this research.

magnetic tensors of large free radicals. *J. Chem. Theory Comput.* 4, 751–764. doi: 10.1021/ct800034c

- Bauernschmitt, R., and Ahlrichs, R. (1996). Treatment of electronic excitations within the adiabatic approximation of time dependent density functional theory. *Chem. Phys. Lett.* 256, 454–464. doi: 10.1016/0009-2614(96)00440-X
- Becke, A. D. (1993). Density-functional thermochemistry. III. The role of exact exchange. *J. Chem. Phys.* 98, 5648–5652. doi: 10.1063/1.464913

- Bhasikuttan, A. C., Suzuki, M., Nakashima, S., and Okada, T. (2002). Ultrafast fluorescence detection in tris(2,2'-bipyridine)ruthenium(II) complex in solution: Relaxation dynamics involving higher excited states. *J. Am. Chem. Soc.* 124, 8398–8405. doi: 10.1021/ja026135h
- Bixon, M., and Jortner, J. (1968). Intramolecular radiationless transitions. *J. Chem. Phys.* 48, 715–726. doi: 10.1063/1.1668703
- Carey, M. C., Adelman, S. L., and McCusker, J. K. (2019). Insights into the excited state dynamics of Fe(II) polypyridyl complexes from variable-temperature ultrafast spectroscopy. *Chem. Sci.* 10, 134–144. doi: 10.1039/C8SC04025G
- Catone, D., O'Keefe, P., Satta, M., Paladini, A., Ciavardini, A., Toschi, F., et al. (2018). A combined theoretical and experimental study of the ultrafast photophysics of Rhodamine B. *Mol. Phys.* 116, 2162–2171. doi: 10.1080/00268976.2018.1464670
- Catone, D., Stener, M., Decleva, P., Contini, G., Zema, N., Prosperi, T., et al. (2012). Resonant circular dichroism of chiral metal-organic complex. *Phys. Rev. Lett.* 108, 83001. doi: 10.1103/PhysRevLett.108.083001
- Catone, D., Turchini, S., Stener, M., Decleva, P., Contini, G., Prosperi, T., et al. (2013). Photoelectron spectroscopy and circular dichroism of a chiral metal-organic complex. *Rend. Lincei.* 24, 269–275. doi: 10.1007/s12210-013-0245-1
- Chergui, M. (2018). Ultrafast photophysics and photochemistry of iron hexacyanides in solution: Infrared to X-ray spectroscopic studies. *Coord. Chem. Rev.* 372, 52–65. doi: 10.1016/j.ccr.2018.05.021
- Damrauer, N. H., Cerullo, G., Yeh, A., Boussie, T. R., Shank, C. V., and McCusker, J. K. (1997). Femtosecond dynamics of excited-state evolution in [Ru(bpy)₃]²⁺. *Science* 275, 54–57. doi: 10.1126/science.275.5296.54
- Demtröder, W. (2008). *Laser Spectroscopy Vol. 2: Experimental Techniques*. Berlin Heidelberg: Springer-Verlag.
- Francl, M. M., Pietro, W. J., Hehre, W. J., Binkley, J. S., Gordon, M. S., DeFrees, D. J., et al. (1982). Self-consistent molecular orbital methods. XXIII. A polarization-type basis set for second-row elements. *J. Chem. Phys.* 77, 3654–3665. doi: 10.1063/1.444267
- Fratoddi, I., Cartoni, A., Venditti, I., Catone, D., O'Keefe, P., Paladini, A., et al. (2018). Gold nanoparticles functionalized by rhodamine B isothiocyanate: a new tool to control plasmonic effects. *J. Colloid Interf. Sci.* 513, 10–19. doi: 10.1016/j.jcis.2017.11.010
- Frisch, M. J., Trucks, G. W., Schlegel, H. B., Scuseria, G. E., Robb, M. A., Cheeseman, J. R. et al. (2016). *Gaussian09, Revision A.02*. Wallingford CT: Gaussian, Inc.
- Fujisaki, H., Zhang, Y., and Straub, J. E. (2006). Time-dependent perturbation theory for vibrational energy relaxation and dephasing in peptides and proteins. *J. Chem. Phys.* 124, 144910. doi: 10.1063/1.2191038
- Griffith, J. S. (1961). *The Theory of Transition-Metal Ions*. London: Cambridge University Press.
- Grossmann, F. (2013). *Theoretical Femtosecond Physics: Atoms and Molecules in Strong Laser Fields*. Berlin Heidelberg: Springer-Verlag Springer.
- Hariharan, P. C., and Pople, J. A. (1973). The influence of polarization functions on molecular orbital hydrogenation energies. *Theor. Chim. Acta* 28, 213–222. doi: 10.1007/BF00533485
- Hsu, C. C., Lin, C. C., Chou, P. T., Lai, C. H., Hsu, C. W., Lin, C. H., et al. (2012). Harvesting highly electronically excited energy to triplet manifolds: state-dependent intersystem crossing rate in Os(II) and Ag(I) complexes. *J. Am. Chem. Soc.* 134, 7715–7724. doi: 10.1021/ja2107788
- Huse, N., Cho, H., Hong, K., Jamula, L., de Groot, F. M. F., Kim, T. K., et al. (2011). Femtosecond Soft X-ray spectroscopy of solvated transition-metal complexes: deciphering the interplay of electronic and structural dynamics. *J. Phys. Chem. Lett.* 2, 880–884. doi: 10.1021/jz200168m
- Ishii, Y., Iwahama, T., Sakaguchi, S., Nakayama, K., and Nishiyama, Y. (1996). Alkane oxidation with molecular oxygen using a new efficient catalytic system: N-Hydroxyphthalimide (NHPI) Combined with Co(acac)_n (n = 2 or 3). *J. Org. Chem.* 61, 4520–4526. doi: 10.1021/JO951970L
- Juban, E. A., and McCusker, J. K. (2005). Ultrafast dynamics of ²E state formation in Cr(acac)₃. *J. Am. Chem. Soc.* 127, 6857–6865. doi: 10.1021/ja042153i
- Lee, C., Yang, W., and Parr, R. G. (1988). Development of the Colle-Salvetti correlation-energy formula into a functional of the electron density. *Phys. Rev. B* 37, 785–789. doi: 10.1103/PhysRevB.37.785
- Liu, C., Zhang, J., Lawson Daku, L. M., Gosztola, D., Canton, S. E., and Zhang, X. (2017). Probing the impact of solvation on photoexcited spin crossover complexes with high-precision X-ray transient absorption spectroscopy. *J. Am. Chem. Soc.* 139, 17518–17524. doi: 10.1021/jacs.7b09297
- Maçóas, E. M., Kananavicius, R., Myllyperkiö, P., Pettersson, M., and Kunttu, H. (2007). Relaxation dynamics of Cr(acac)₃ probed by ultrafast infrared spectroscopy. *J. Am. Chem. Soc.* 129, 8934–8935. doi: 10.1021/ja071859k
- McCusker, J. K. (2003). Femtosecond absorption spectroscopy of transition metal charge-transfer complexes. *Acc. Chem. Res.* 36, 876–887. doi: 10.1021/AR030111D
- McCusker, J. K., Walda, K. N., Magde, D., and Hendrickson, D. N. (1993). Picosecond excited-state dynamics in octahedral cobalt(III) complexes: intersystem crossing versus internal conversion. *Inorg. Chem.* 32, 394–399. doi: 10.1021/ic00056a010
- Monat, J. E., and McCusker, J. K. (2000). Femtosecond excited-state dynamics of an iron(II) polypyridyl solar cell sensitizer model. *J. Am. Chem. Soc.* 122, 4092–4097. doi: 10.1021/ja992436o
- Prier, C. K., Rankic, D. A., and MacMillan, D. W. C. (2013). Visible light photoredox catalysis with transition metal complexes: applications in organic synthesis. *Chem. Rev.* 113, 5322–5363. doi: 10.1021/cr300503r
- Ruggiero, E., Alonso-de Castro, S., Habtemariam, A., and Salassa, L. (2014). “The photochemistry of transition metal complexes and its application in biology and medicine,” in *Luminescent and Photoactive Transition Metal Complexes as Biomolecular Probes and Cellular Reagents. Structure and Bonding*, ed K. W. Lo, (Heidelberg; New York, NY; Dordrecht; London: Springer Verlag) 69–107.
- Savarese, M., Aliberti, A., De Santo, I., Battista, E., Causa, F., Netti, P. A., and Rega, N. (2012). Fluorescence lifetimes and quantum yields of rhodamine derivatives: new insights from theory and experiment. *J. Phys. Chem. A* 116, 7491–7497. doi: 10.1021/jp3021485
- Savarese, M., Raucci, U., Adamo, C., Netti, P. A., Ciofini, I., and Rega, N. (2014). Non-radiative decay paths in rhodamines: new theoretical insights. *Phys. Chem. Chem. Phys.* 16, 20681–20688. doi: 10.1039/C4CP02622E
- Scalmani, G., and Frisch, M. J. (2010). Continuous surface charge polarizable continuum models of solvation. I. General formalism. *J. Chem. Phys.* 132, 114110. doi: 10.1063/1.3359469
- Squibb, R. J., Sapunar, M., Ponzi, A., Richter, R., Kivimäki, A., Plekan, O., et al. (2018). Acetylacetone photodynamics at a seeded free-electron laser. *Nat. Commun.* 9, 63. doi: 10.1038/s41467-017-02478-0
- Stephens, P. J., Devlin, F. J., Chabalowski, C. F., and Frisch, M. J. (1994). Ab Initio calculation of vibrational absorption and circular dichroism spectra using density functional force fields. *J. Phys. Chem.* 98, 11623–11627. doi: 10.1021/j100096a001
- Tomasi, J., Mennucci, B., and Cammi, R. (2005). Quantum mechanical continuum solvation models. *Chem. Rev.* 105, 2999–3094. doi: 10.1021/cr9904009
- Tramer, A., Jungen, C., and Lahmani, F. (2010). *Energy Dissipation in Molecular Systems*. Berlin Heidelberg: Springer-Verlag.
- Valiev, R. R., Cherepanov, V. N., Baryshnikov, G. V., and Sundholm, D. (2018). First-principles method for calculating the rate constants of internal-conversion and intersystem-crossing transitions. *Phys. Chem. Chem. Phys.* 20, 6121–6133. doi: 10.1039/C7CP08703A
- Vlček, A. (2000). The life and times of excited states of organometallic and coordination compounds. *Coord. Chem. Rev.* 200–202, 933–977. doi: 10.1016/S0010-8545(00)00308-8

- Vosko, S. H., Wilk, L., and Nusair, M. (1980). Accurate spin-dependent electron liquid correlation energies for local spin density calculations: a critical analysis. *Can. J. Phys.* 58, 1200–1211. doi: 10.1139/p80-159
- Wada, O. (2004). Femtosecond all-optical devices for ultrafast communication and signal processing. *New J. Phys.* 6, 183. doi: 10.1088/1367-2630/6/1/183
- Wada, S., and Tanaka, K. (2013). “Chemical Reactions Induced by Core Electron Excitations,” in *Fundamentals of Mass Spectrometry*, eds. K. Hiraoka (New York: Springer New York), 61–79.
- Wagenknecht, P. S., and Ford, P. C. (2011). Metal centered ligand field excited states: their roles in the design and performance of transition metal based photochemical molecular devices. *Coord. Chem. Rev.* 255, 591–616. doi: 10.1016/j.CCR.2010.11.016

Conflict of Interest Statement: The authors declare that the research was conducted in the absence of any commercial or financial relationships that could be construed as a potential conflict of interest.

The handling editor declared a past co-authorship with one of the authors DC.

Copyright © 2019 Ferrari, Satta, Palma, Di Mario, Catone, O’Keeffe, Zema, Prospero and Turchini. This is an open-access article distributed under the terms of the Creative Commons Attribution License (CC BY). The use, distribution or reproduction in other forums is permitted, provided the original author(s) and the copyright owner(s) are credited and that the original publication in this journal is cited, in accordance with accepted academic practice. No use, distribution or reproduction is permitted which does not comply with these terms.